Łukasiewicz
Institute of Aviation

DOI: 10.2478/fas-2025-0007
FATIGUE OF AIRCRAFT STRUCTURES
Volume 2025: Issue 17, pp. 99-116

DEFECT DETECTABILITY IN CFRP COMPOSITES USING LONG PULSE THERMOGRAPHY: A COMPARATIVE STUDY OF FIVE DEFECT TYPES

Patryk Ciężak[1*] 0000-0002-7389-7109
Paulina Kamińska[2] 0000-0001-6414-559X
Marcin Kurdelski[2] 0000-0003-3461-1865
Jakub Kotowski[2] 0000-0003-3795-242X
Piotr Synaszko[2] 0000-0002-7884-0582
Andrzej Leski[1,3] 0000-0003-3006-8877

[1] Mechanical Department, Military University of Technology, 2 Sylwestra Kaliskiego Str., 00-908 Warsaw, Poland
[2] Aircraft Airworthiness Division, Air Force Institute of Technology, 6 Księcia Bolesława Str., 01-494 Warsaw, Poland
[3] Łukasiewicz Research Network – Institute of Aviation, 110/114 Krakowska Ave., 02-256 Warsaw, Poland

Abstract

This study investigates the applicability of Long Pulse Thermography (LPT) for detecting artificial defects in carbon-fiber-reinforced polymer (CFRP) composites. The work aimed to determine which types of defects can be detected in a CFRP panel using active infrared thermography and to assess the influence of defect type, size, and depth on their detectability. The test specimen was a CFRP laminate manufactured from unidirectional prepreg using the autoclave process. The panel had a variable thickness, and artificial defects were introduced at different locations to simulate typical manufacturing- and service-related damage. The investigated defects included: prepreg foil, simulating interlayer insertion caused by errors during prepreg lay-up; flat-bottom holes, simulating delamination caused, for example, by low-energy impacts; paper inserts, simulating interlayer insertion caused by the inclusion of a foreign body during manufacturing; flat-bottom holes filled with epoxy resin, simulating resin-rich areas; and graphite foil, simulating interlayer insertion defects. Thermographic measurements were performed using long-pulse thermal excitation, and the thermal response was analyzed during the cooling phase. The results showed that defect detectability depended strongly on defect type and increased with increasing defect diameter. Flat-bottom holes and resin-rich defects produced the clearest thermal indications and the highest detection repeatability, whereas prepreg foil and paper inserts yielded less distinct signals, particularly for smaller diameters. Under the applied test conditions, graphite foil inserts were not detected. The results confirm that LPT is a promising non-destructive testing method for the rapid inspection of CFRP structures; however, its effectiveness is limited for defects generating low thermal contrast.

Keywords: non-destructive testing (NDT); thermography (IRT); composite; Long Pulse Thermography (LPT).

* Corresponding author. Email address: patrykciezak@gmail.com
Received 10.04.2026 • Revised 27.04.2026 • Accepted 30.04.2026
Article category: research article

1. INTRODUCTION

The use of composite materials in modern aircraft structures has increased significantly over recent decades. Major aerospace manufacturers such as Airbus and Boeing have incorporated a large proportion of composites into their latest airframes to reduce structural weight while maintaining high mechanical performance and corrosion resistance. A representative example is the Boeing 787, in which composites account for approximately 50% of the structural weight, while aluminum, titanium, steel, and other materials represent 20%, 15%, 10%, and 5%, respectively (Restrepo-Girón & Loaiza-Correa, 2016; Balageas et al., 2016; Alemour et al., 2019; Kamińska et al., 2019). In aerospace applications, a wide range of composite systems are used, including glass-, carbon-, aramid-, and boron-fiber-reinforced materials, as well as different structural configurations such as GLARE, sandwich structures, and monolithic laminates.

The increasing share of composites in aircraft structures creates a growing demand for reliable non-destructive inspection (NDI) methods capable of detecting both manufacturing flaws and in-service damage. In the case of large-area composite components, shearography and thermography are among the most commonly applied inspection techniques. However, shearography is mainly sensitive to defects that produce surface deformation under loading and may therefore be less effective for detecting subsurface discontinuities in laminates that do not generate measurable out-of-plane deformation. For this reason, active infrared thermography is considered a promising alternative for the inspection of composite materials.

Among active thermographic techniques, LPT offers significant potential for the evaluation of CFRP structures. By applying relatively long thermal excitation and analyzing the transient thermal response, this method enables the detection of subsurface defects that locally disturb heat flow in the material. As a result, LPT can be used to identify defects of different origins and morphologies in composite laminates.

Previous studies have shown that long-pulse and related step-heating thermographic methods can be used for defect detection, depth evaluation, and quantitative damage assessment in composite materials (Balageas & Roche, 2014; Roche & Balageas, 2015; Almond et al., 2017; Kalyanavalli et al., 2018; Wang et al., 2018, 2022; Zhuo et al., 2023;). Almond et al. (2017) discussed long-pulse excitation for thermographic NDE, Kalyanavalli et al. (2018) investigated long-pulse thermography for fiber-reinforced composites, and Wang et al. (2018, 2022) demonstrated the relevance of LPT for defect-depth evaluation and image-processing-based damage assessment in composites. These studies confirm the potential of active thermography, but they also indicate that detectability depends on defect type, depth, size, and thermophysical contrast; therefore, comparative tests on different artificial defect classes remain necessary for practical CFRP inspection.

This study aimed to assess the effectiveness of LPT in detecting artificial defects in a CFRP laminate and to compare how well different defect types introduced into the material can be detected. The investigated defects simulated typical manufacturing- and service-related discontinuities, including interlayer insertions, delamination, and resin-rich areas. Particular attention was paid to the influence of defect type and size on the

visibility of thermal indications. The novelty of the study lies in the comparative assessment of defect detectability for several types of simulated subsurface defects embedded in a CFRP panel of variable thickness under identical experimental conditions. The results provide practical information on the capabilities and limitations of LPT for the non-destructive inspection of composite aircraft structures.

2. LONG PULSE THERMOGRAPHY (LPT)

LPT is an active NDT technique used to detect subsurface defects in materials, particularly in complex multi-layered structures (Maldague, 2001a, 2001b; Balageas & Roche, 2014; Pedrayes et al., 2022). In LPT, a low-intensity optical heat source is applied for a relatively long period, and the surface temperature field is recorded using an infrared camera. Subsurface defects are detected because they disturb heat flow and therefore modify the transient thermal response recorded at the inspected surface (Vavilov & Burleigh, 2015; Almond et al., 2017; Kalyanavalli et al., 2018; Wang et al., 2018; Manohar & di Scalea, 2013).

2.1. Principle of long-pulse thermal excitation

Compared with short-pulse thermography, the longer heating period used in LPT can improve sensitivity to defects located deeper below the surface because more thermal energy is introduced into the laminate. Thermal contrast is then evaluated primarily during the cooling phase, when local differences in thermal diffusivity, thermal conductivity, and heat capacity influence the rate of temperature decay (Almond et al., 2017; Kalyanavalli et al., 2018; Huang et al., 2022).

2.2. Relationship between LPT and Step Heating Thermography

Step Heating Thermography (SHT) uses a gradual or rectangular heating input and records the temperature evolution during and after heating (Balageas & Roche, 2014; Roche & Balageas, 2015; Zhuo et al., 2023). LPT can be regarded as a long-pulse implementation of active thermography in which the excitation resembles a step-heating input; however, the analysis in the present work focuses on the post-heating transient cooling response rather than on a steady-state temperature rise. Therefore, the experimental setup may be described as SHT-type excitation combined with LPT analysis: SHT defines the heating input, whereas LPT defines the post-excitation transient evaluation used to assess defect detectability.

2.3. Applications in aerospace and composite inspection

Both LPT and SHT are used in aerospace, automotive, and manufacturing applications where safety and structural integrity are critical (Carslaw & Jaeger, 1959; Maldague, 2001b; Vedula, 2010). Their non-contact and non-invasive character makes them suitable for inspecting composite parts, bonded joints, and layered structures without damaging the component (Shepard, 2003; Sun, 2006; Kalyanavalli et al., 2018; Wang et al., 2018).

2.4. Data processing developments

Recent advances in SHT and related active thermographic methods include the use of Thermographic Signal Reconstruction (TSR), early detection and characterization procedures, and virtual heat-flux reconstruction (Favro et al., 1995; Deák & Czigány, 2009; Świderski & Vavilov, 2009; Manohar & di Scalea, 2013; Balageas & Roche, 2014; Ghadermazi et al., 2015; Zhuo et al., 2023). These approaches improve defect contrast, reduce noise, and support quantitative interpretation of thermal sequences.

For the present study, the important implication is that post-processing can enhance defect visibility, but the final detectability of a defect still depends on its geometry, embedded depth, and thermophysical mismatch with the surrounding CFRP laminate (Carslaw & Jaeger, 1959; Ringermacher et al., 1998; Almond & Pickering, 2012; Wang et al., 2022).

Building on these principles, the following section describes the specimen design and experimental procedure used to evaluate LPT performance across five defect classes.

3. EXPERIMENTAL VALIDATION

3.1. Specimen information

The specimen, with dimensions of 850 × 450 mm, was manufactured from a unidirectional carbon-fiber/epoxy prepreg (CFRP UD) cured in an autoclave. The material system therefore represents a typical aerospace CFRP laminate with continuous UD carbon reinforcement and an epoxy matrix. Additional/foreign elements used to simulate defects included prepreg foil, paper inserts (Figure 1) and graphite foil.

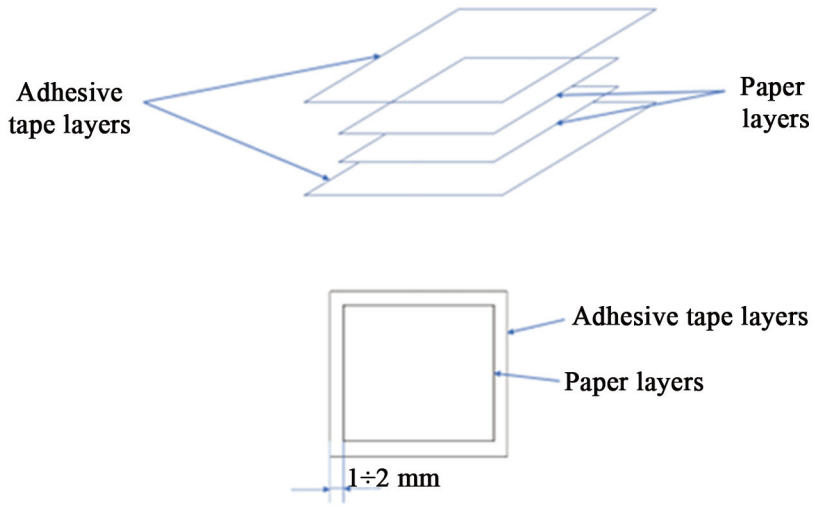

Figure 1. Paper inserts used to simulate interlayer foreign-body inclusions.

The specimen contained five types of defects, simulating three types of composite damage:

- Row 1 – prepreg foil (simulates interlayer insertion, a manufacturing defect caused by the worker placing the prepreg layers in the mold, Figure 2);
- Row 2 – flat-bottom holes (simulate delamination caused, for example, by low-energy impacts, Figure 2);
- Row 3 – paper inserts (simulate interlayer insertion caused by the inclusion of a foreign body, e.g., a piece of nitrile glove, in the structure during the laying of layers in the mold at the production stage, Figure 2);
- Row 4 – flat-bottom holes filled with epoxy resin (simulate resin-rich areas, Figure 2);
- Row 5 – graphite foil (simulates interlayer insertion, a manufacturing defect caused by the worker placing the prepreg layers in the mold, Figure 2).

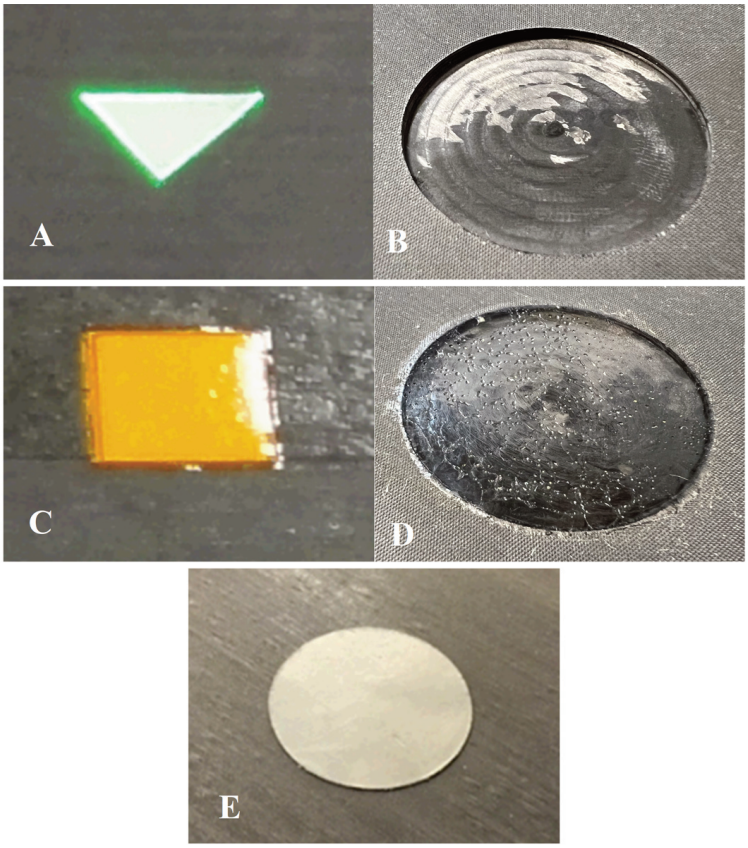

Figure 2. A – Prepreg foil; B – Flat-bottom hole; C – Paper insert; D – Flat-bottom hole filled with epoxy resin; E – Graphite foil.

The triangular planform of defect A and the square planform of defect C were intentionally selected to distinguish insert-type defects from the circular flat-bottom holes and to verify whether non-circular geometries could be reproduced in the thermal indication. The remaining defects were circular because they were manufactured as drilled flat-bottom holes or circular inserts. In LPT images, lateral heat diffusion tends to smooth sharp boundaries; therefore, triangular and square defects may appear as rounded thermal footprints during post-processing.

The specimen was a carbon composite plate of variable thickness. Based on thickness, the specimen can be divided into three zones:

- Zone 1 – 16 layers;
- Zone 2 – transitional;
- Zone 3 – 24 layers.

Holes and inclusions simulating defects were placed in all three zones. Zones 1 and 3 each contain 25 defects arranged in 5 rows and 5 columns. The transitional zone contains 10 defects arranged in 5 rows and 2 columns. Photographs of the specimen from both sides, detailing the transition zone, are shown in Figure 3. A schematic diagram of the specimen is shown in Figure 4.

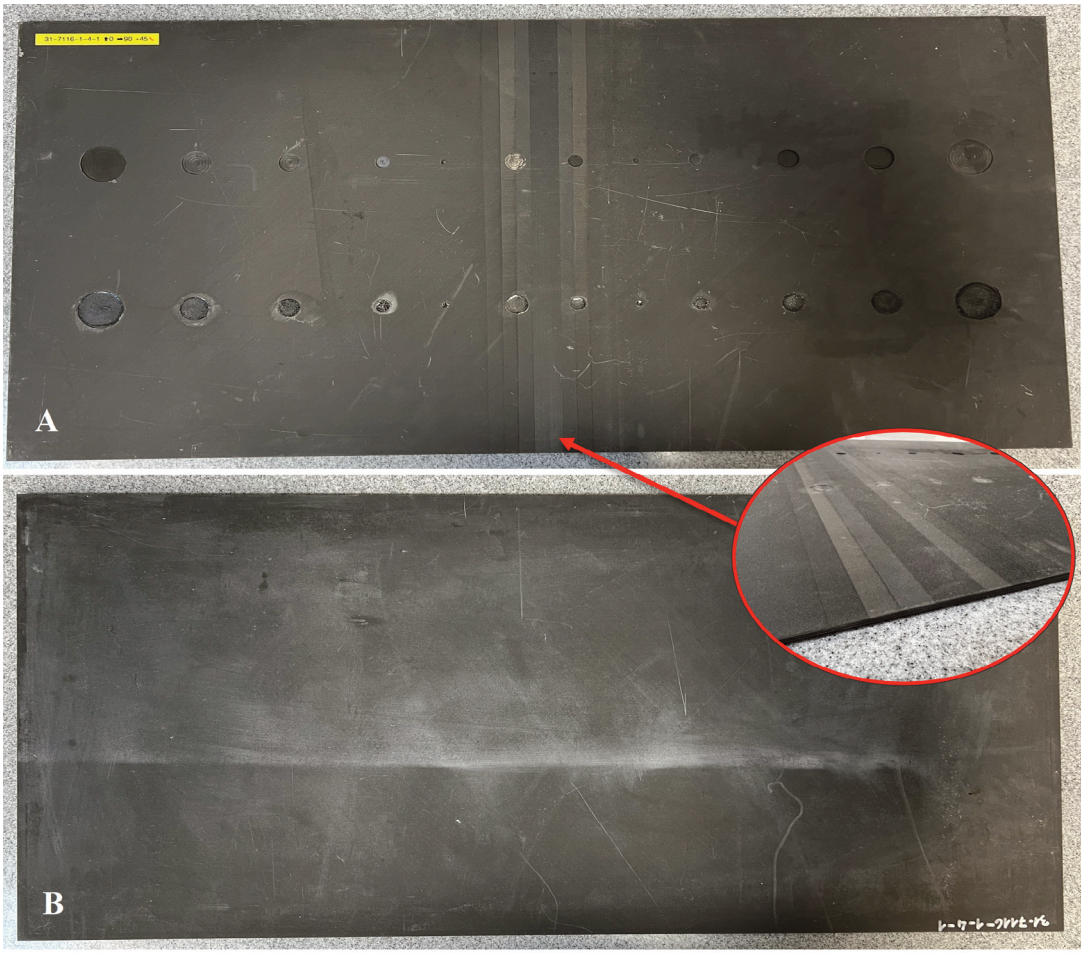

Figure 3. Photographs of the specimen (A – bottom side, B – top side).

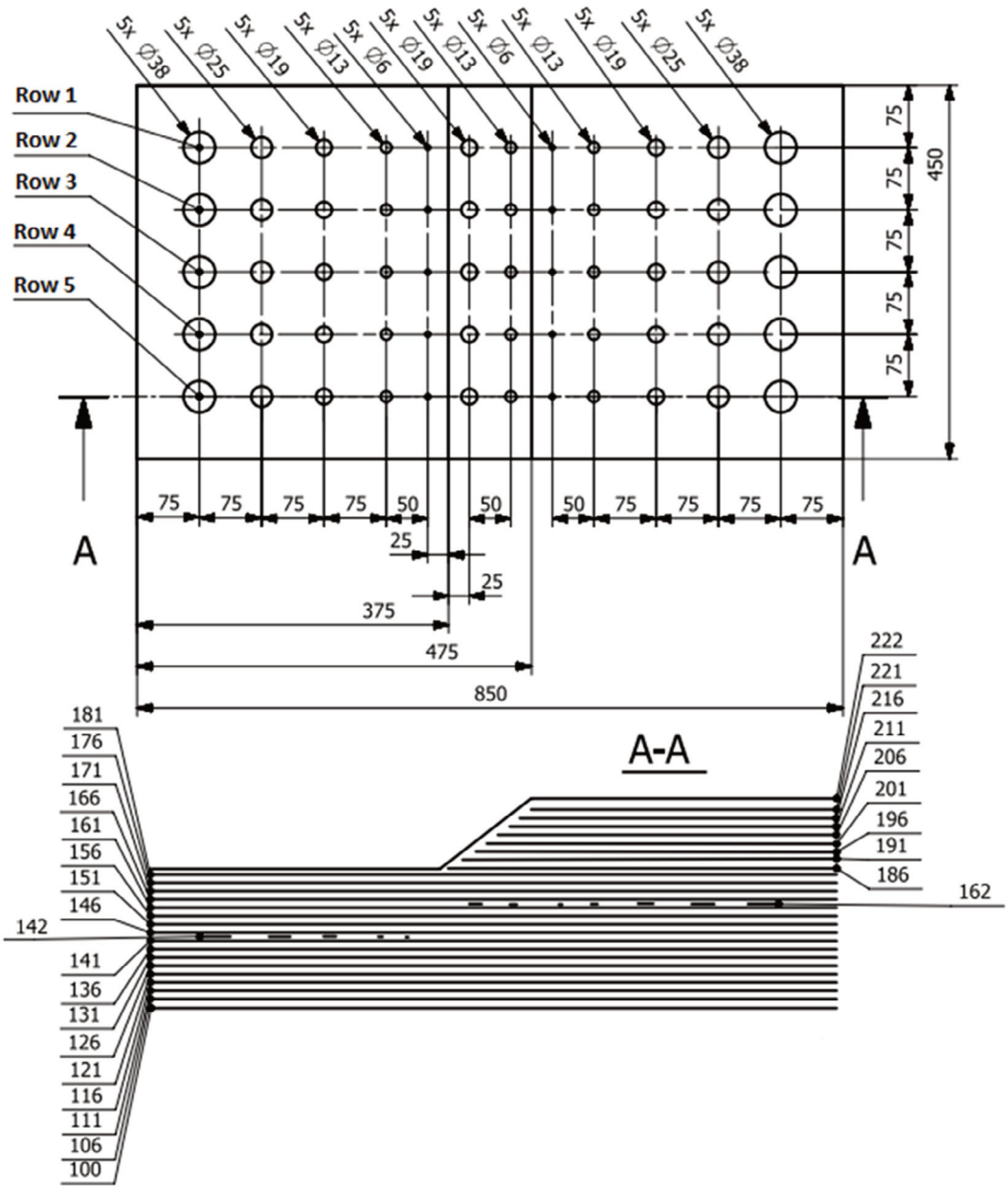

Figure 4. Schematic diagram of the specimen.

The specimen was manufactured using the autoclave process, following the thermal cycle shown in Figure 5.

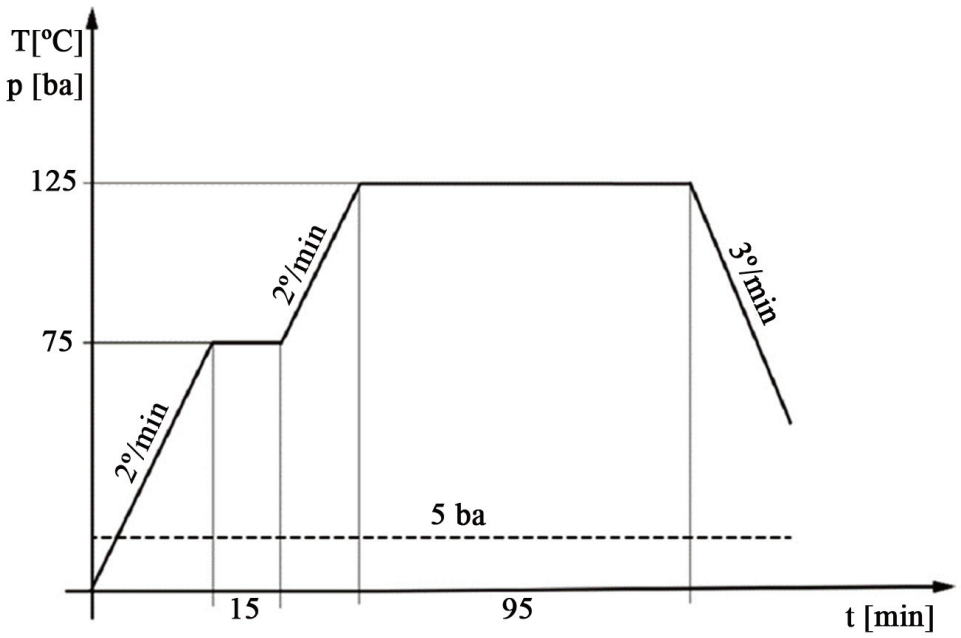

Figure 5. Heating cycle graph for specimen manufacturing.

3.2. Experimental process and thermographic setup

The experiment used a rectangular long-pulse excitation. From the system point of view, this corresponds to the SHT excitation mode available in the C-CheckIR system; from the data-analysis point of view, the inspection was evaluated as LPT because the defect response was assessed primarily during the transient cooling phase after heating. Thus, SHT and LPT are not separate inspections in this work: SHT describes the heating input, whereas LPT describes the post-excitation transient analysis. The specimen, with dimensions of 850 × 450 mm, was divided into four test areas because the field of view of the C-CheckIR device is 430 × 340 mm at an operating distance of 400 mm. The sensor head stimulated the test area with an optical excitation source (halogen lamp) of 2.2 kW at 230 V. The standoff distance of the heat source was selected to avoid local heat concentration and to provide nearly uniform thermal stimulation over the inspected surface. The camera used was an Automation Technology GmbH IRS-336 infrared camera with a maximum resolution of 640 × 512 pixels, a frame rate of 60 Hz, and thermal sensitivity below 30 mK. The camera was positioned so that only the test specimen was visible, in order to minimize reflections from the surrounding area. Thermal image sequences were acquired using irNDT-Mobile and analyzed with the Pulse/Transient Measurement module, which processes the time-dependent temperature response after excitation. The Lock-In Evaluation module is also available in the software for phase and amplitude evaluation of periodically modulated thermal data; however, the present detectability assessment used the transient cooling response after long-pulse heating. The measurement system is shown schematically in Figure 6.

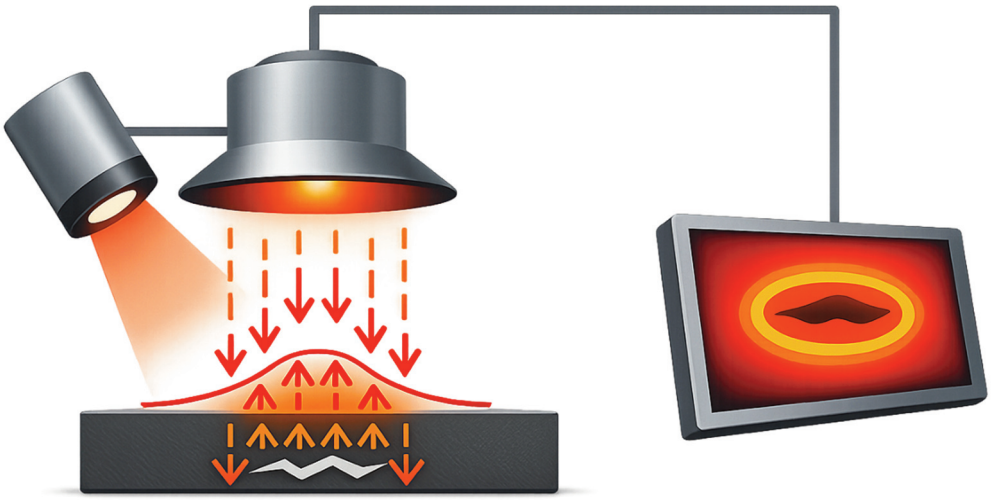

Figure 6. Schematic diagram of the thermography test configuration.

Figure 7 shows a photograph of the C-CheckIR. The system comprises a control unit with software, a testing unit (infrared camera, excitation source, and stand), and connecting cables.

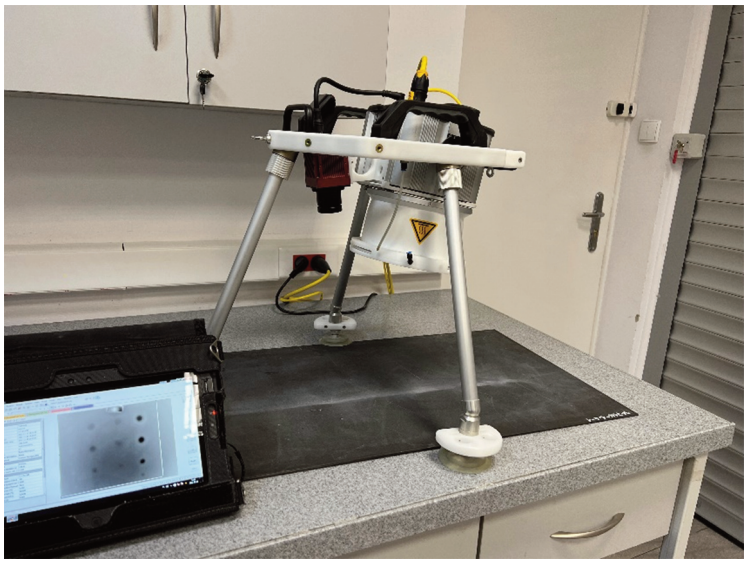

Figure 7. Photograph of the C-CheckIR system during specimen testing.

The acquisition and excitation settings used in the experiment are listed in Tables 1 and 2.

In Table 1, Sync Mode describes how image acquisition was triggered; Free Run indicates that the camera recorded continuously without an external synchronization trigger. Acquisition Duration is the total recording time of the thermal sequence, and Acquisition Frame Rate is the number of infrared frames recorded per second. In Table 2, Rect. Modulation denotes a rectangular on/off heating signal; Amplitude Low and

Amplitude High define the relative lamp power levels; Excitation Period is the complete modulation cycle; Duty Time is the active heating duration within that cycle; and the Rising and Falling Ramp Times smooth the transition between power levels. The number of measurements corresponds to the total number of recorded frames, whereas the Best Results Measurement identifies the frame selected as providing the most interpretable defect contrast.

Table 1. Acquisition parameters.

Parameters	**Value**
Sync Mode	Free run
Acquisition duration	120 [s]
Acquisition frame rate	5 [Hz]

Table 2. Excitation parameters.

Parameters	**Value**
Modulation	Rect.
Amplitude low	0 [%]
Amplitude high	90 [%]
Excitation period	120 [s]
Duty time	10 [s]
Rising ramp time	0.8 [s]
Falling ramp time	0.8 [s]
Number of measurements	359
Best results measurement	346

4. EXPERIMENTAL RESULTS

All results discussed in this section were obtained using LPT analysis of the transient cooling response. Each artificial defect location was measured four times, and the mean, median, and standard deviation were used to evaluate detectability, sizing accuracy, and repeatability. Representative thermal responses are shown in Figure 8, and the spatial distribution of nominal and measured dimensions is summarized in Figure 9.

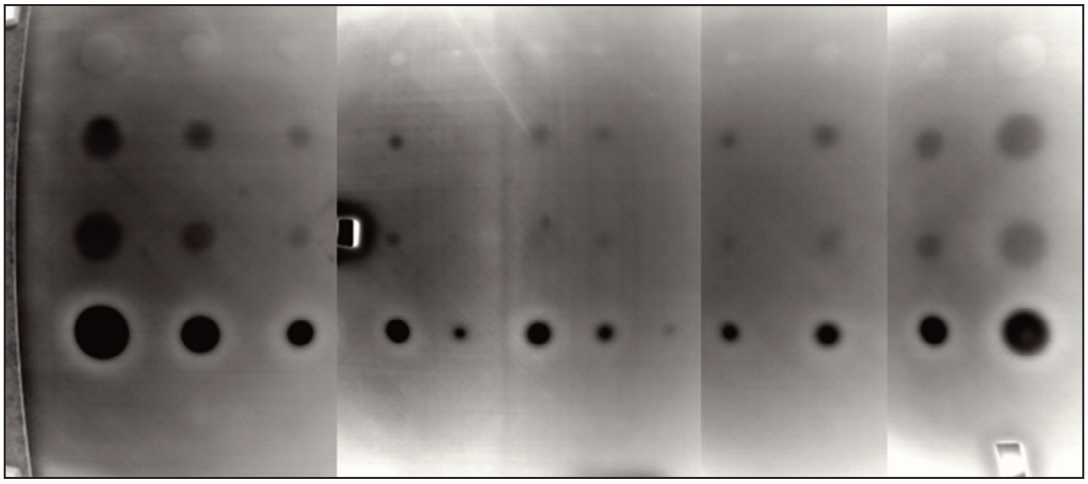

Figure 8. Representative LPT response of the CFRP panel. The five rows correspond to the defect classes defined in Figure 2: Row 1 – prepreg foil; Row 2 – flat-bottom holes; Row 3 – paper inserts; Row 4 – flat-bottom holes filled with epoxy resin; Row 5 – graphite foil. The displayed indications represent thermographic footprints of equivalent-diameter responses; lateral heat diffusion smooths the triangular and square geometries, which is why the indications do not reproduce sharp non-circular edges.

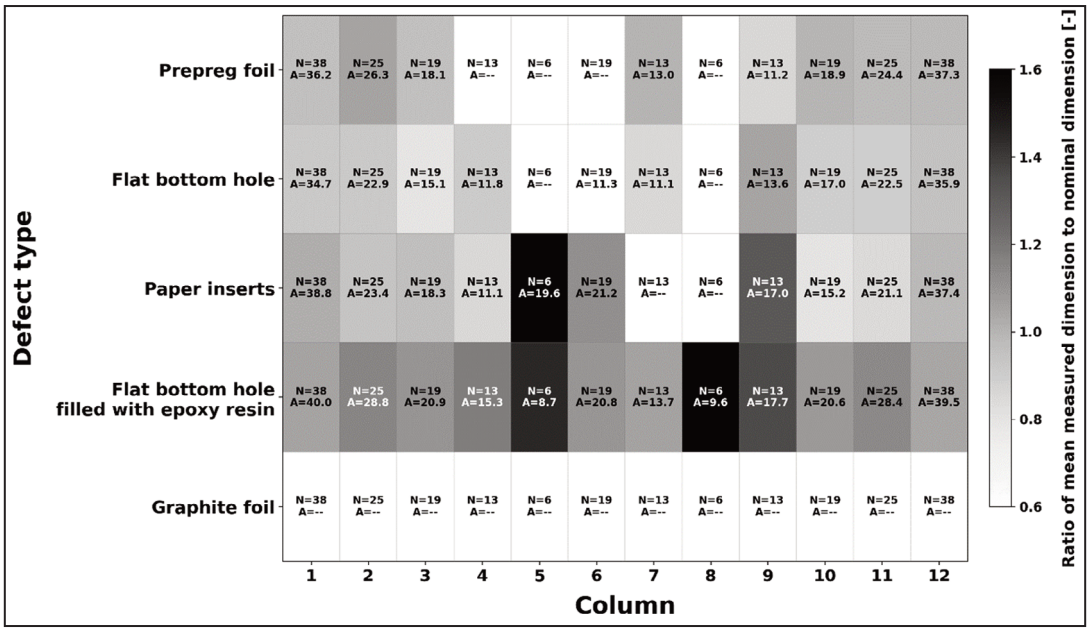

Figure 9. Distribution of defects and mean measured dimensions in the panel grid. Each cell contains the nominal dimension (N) and the mean measured dimension (A). The grayscale background represents the ratio A/N, indicating whether a defect was underestimated, accurately reproduced, or overestimated by LPT.

4.1. Experimental results and error analysis

The LPT results reveal a pronounced dependence of detectability on defect type. The highest detection rate was obtained for flat-bottom holes filled with epoxy resin, for which all 12 defects were identified, corresponding to 100% detectability. This defect class also exhibited the most stable response, with the lowest mean standard deviation of 0.92 mm. At the opposite extreme, graphite foil remained undetected at all 12 locations, indicating that, under the present LPT configuration, this defect class produced insufficient thermal contrast relative to the surrounding CFRP.

The intermediate classes showed distinct error patterns. Prepreg foil was detected in 8 out of 12 cases (66.7%); once detected, it produced a mean error of only −0.58 mm (−2.9%), indicating that defect size was reproduced relatively accurately when a measurable response existed. Flat-bottom holes were detected in 10 out of 12 cases (83.3%), yet their dimensions were systematically underestimated, with a mean error of −2.61 mm (−12.4%) and a mean measured-to-nominal ratio of 0.88. Paper inserts were also detected in 10 out of 12 cases (83.3%), but this group showed the most unstable sizing behavior. The overall mean relative error was +21.0%, although this value was strongly influenced by an outlier at the 6 mm location, where a mean measured size of 19.63 mm was obtained. This result is best interpreted as an anomalous or merged indication rather than a physically realistic size estimate. Flat-bottom holes filled with epoxy resin were not only detected in all cases, but also systematically overestimated. The mean sizing error for this group was +2.51 mm (+19.3%), and the corresponding mean measured-to-nominal ratio reached 1.19. In practical terms, LPT was highly sensitive to resin-rich features, but the thermographic footprint extended beyond the nominal geometrical boundary of the defect. The overall detectability ranking can therefore be expressed as: flat-bottom holes filled with epoxy resin > flat-bottom holes ≈ paper inserts > prepreg foil >>> graphite foil.

Table 3. Summary of LPT detectability, sizing error, and repeatability by defect type.

Defect type	Detected / total	Detection rate [%]	Mean error [mm]	Mean error [%]	Mean SD [mm]
Prepreg foil	8 / 12	66.7	−0.58	−2.9	1.41
Flat bottom hole	10 / 12	83.3	−2.61	−12.4	1.33
Paper inserts	10 / 12	83.3	0.82	21.0	0.94
Flat bottom hole filled with epoxy resin	12 / 12	100.0	2.51	19.3	0.92
Graphite foil	0 / 12	0.0	—	—	—

Table 3 confirms that detectability and accuracy are not equivalent. For example, prepreg foil exhibited a lower detection rate than flat-bottom holes, but once detected it was sized more accurately. Conversely, flat-bottom holes filled with epoxy resin achieved the best detectability and repeatability, although they were consistently oversized. This distinction is important for NDT practice because the best-detected defect is not necessarily the most accurately sized one.

4.2. Effect of depth and dimensions on the defect detection

When all defect classes are considered together, the detection rate increases with nominal size. For 6 mm defects, only 3 out of 10 cases were detected (30.0%); for 13 mm defects, 10 out of 15 (66.7%); for 19 mm defects, 11 out of 15 (73.3%); and for both 25 mm and 38 mm defects, 8 out of 10 (80.0%). These results indicate that the practical detection threshold for the present LPT configuration lies close to 13 mm. Defects of 6 mm are generally below the robust detectability limit, except when the defect class generates particularly strong thermal contrast, as observed for flat-bottom holes filled with epoxy resin. The size-dependent trend is illustrated in Figure 10.

Table 4. Detection rate as a function of nominal defect dimension.

Nominal dimension [mm]	Detected / total	Detection rate [%]
6	3 / 10	30.0
13	10 / 15	66.7
19	11 / 15	73.3
25	8 / 10	80.0
38	8 / 10	80.0

Dimension alone, however, does not fully explain the observed behavior. The defect response also depends strongly on depth and defect character, as reflected by the row-to-row differences defined during specimen fabrication. Figure 11 compares the measured and nominal dimensions for each defect type, and the following local comparisons show that defects of the same nominal dimension can produce different LPT responses. At a nominal dimension of 13 mm, the mean measured size followed the order: prepreg foil (12.08 mm) ≈ flat-bottom hole (12.15 mm) < paper inserts (14.08 mm) < flat-bottom hole filled with epoxy resin (15.58 mm). At 19 mm, the order was: flat-bottom hole (14.46 mm) < paper inserts (18.23 mm) ≈ prepreg foil (18.50 mm) < flat-bottom hole filled with epoxy resin (20.75 mm). At 25 mm: paper inserts (22.26 mm) ≈ flat-bottom hole (22.72 mm) < prepreg foil (25.38 mm) < flat-bottom hole filled with epoxy resin (28.63 mm). At 38 mm: flat-bottom hole (35.30 mm) < prepreg foil (36.72 mm) < paper inserts (38.10 mm) < flat-bottom hole filled with epoxy resin (39.72 mm).

These sequences show that defects of the same nominal diameter may produce substantially different apparent dimensions in LPT, indicating that the thermal signature

is governed by more than geometry alone. The through-thickness position defined in the specimen design, the local stacking sequence, and the thermophysical contrast between the defect and the surrounding laminate all contribute to the final response. This effect is visible in Figure 9 and in the local comparisons between columns. For example, for the 19 mm defects located in column 6, the mean measured size was 11.28 mm for flat-bottom holes, 21.20 mm for paper inserts, and 20.77 mm for flat-bottom holes filled with epoxy resin, whereas the prepreg foil at the same nominal location was not detected. Similarly, for the 13 mm defects in column 9, the mean measured sizes were 11.18 mm for prepreg foil, 13.56 mm for flat-bottom holes, 17.04 mm for paper inserts, and 17.71 mm for flat-bottom holes filled with epoxy resin.

The smallest defects provide the clearest evidence of the combined depth–dimension effect. The 6 mm flat-bottom holes were not detected, nor were the 6 mm prepreg foil or graphite foil inserts, while the 6 mm flat-bottom holes filled with epoxy resin were detected at both locations, with mean measured dimensions of 8.72 mm and 9.63 mm. The only other 6 mm response was the aforementioned 19.63 mm paper-insert indication, which should be interpreted as an anomalous case. Therefore, for small defects, the decisive factor is not merely nominal size, but whether the defect class and its depth placement are capable of generating sufficient thermographic contrast in LPT.

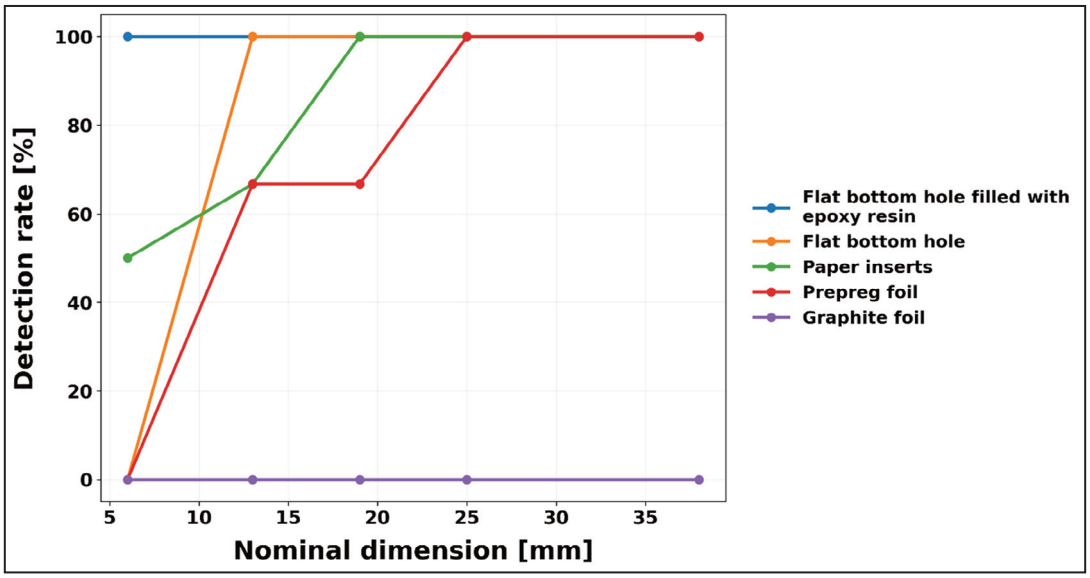

Figure 10. Detection rate as a function of nominal defect dimension for each defect type. The figure shows that 6 mm defects are generally below the robust LPT detectability limit, whereas detectability increases markedly from approximately 13 mm onward.

In summary, the LPT results demonstrate that defect detectability in CFRP is governed by the combined action of nominal dimension, through-thickness location, and defect nature. Flat-bottom holes filled with epoxy resin were the most visible and the most repeatable. Flat-bottom holes and paper inserts showed good but imperfect detectability with different sizing biases, prepreg foil remained moderately detectable but relatively accurate when visible, and graphite foil was effectively invisible under the present test conditions. These observations support the conclusion that defect

detectability in CFRP cannot be characterized by size alone, and that any comparative evaluation of LPT performance must explicitly account for the defect class and its embedded depth.

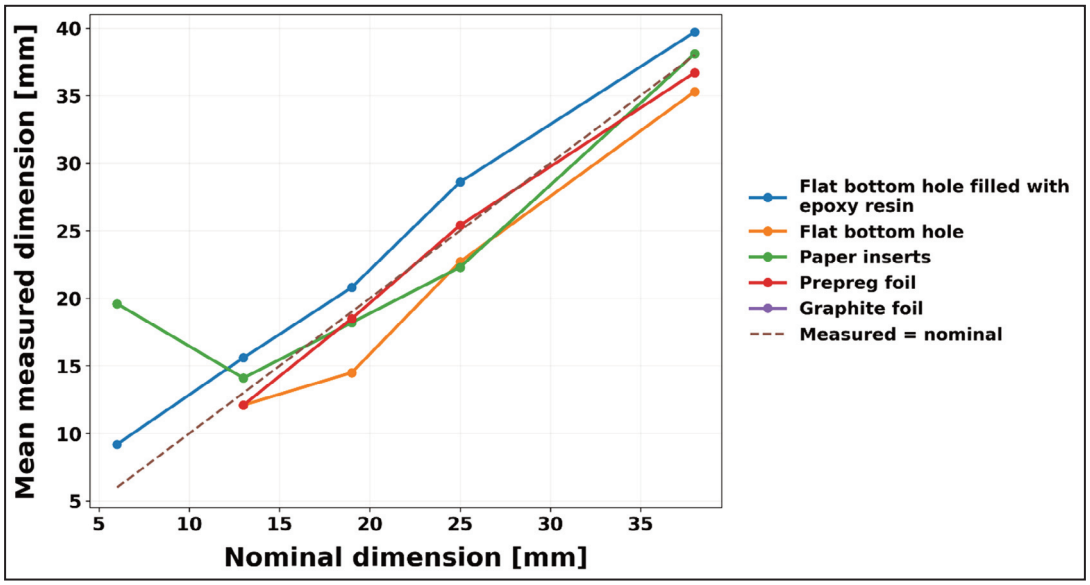

Figure 11. Mean measured dimension versus nominal dimension for each defect type. The diagonal line represents perfect agreement between the measured and nominal dimensions. Flat-bottom holes are predominantly underestimated, whereas flat-bottom holes filled with epoxy resin are systematically overestimated.

5. DISCUSSION

The experimental results raise several points that warrant further physical and practical interpretation.

From a physical perspective, the observed ranking of defect visibility can be attributed to the magnitude of the thermal disturbance introduced by each defect and to the way that disturbance modifies heat flow during cooling. Resin-rich regions and flat-bottom holes produced larger local disturbances than thin graphite inserts, which likely remained insufficiently contrasted thermally under the selected excitation conditions. Consequently, LPT in this configuration is most reliable when the defect produces a clear thermophysical discontinuity rather than only a minor geometrical or material discontinuity.

The results also show that detectability and sizing accuracy should be treated as separate performance criteria. A defect may be readily detectable while still being systematically overestimated or underestimated in size. This effect was particularly evident for flat-bottom holes filled with epoxy resin, which were always detected but consistently oversized, and for flat-bottom holes, which were detected in most cases but systematically underestimated. Paper inserts exhibited the largest variability in size assessment, primarily due to the anomalous response recorded for one of the 6 mm defects. These observations suggest that the apparent thermographic footprint is

governed not only by the geometric size of the defect, but also by the local heat-flow disturbance generated by its material nature and embedded position.

A further important outcome is the strong influence of nominal defect size on LPT performance. In the present experimental configuration, defects of 6 mm were generally below the robust detectability limit, except for resin-rich defects, whereas detectability increased markedly from 13 mm onward. At the same time, local comparisons between defects of identical nominal diameter showed that size alone does not fully explain the thermal response. Differences observed between prepreg foil, flat-bottom holes, paper inserts, and resin-rich defects at the same nominal size confirm that defect class and depth placement play a critical role in shaping the recorded signal. Therefore, any practical evaluation of LPT for CFRP inspection should consider defect morphology and thermophysical contrast in addition to nominal dimensions.

From a practical standpoint, the study indicates that LPT can serve as a useful screening tool for large CFRP components, especially where rapid, non-contact inspection is required. The method is particularly suitable for defects producing clear thermal contrast, but its sensitivity decreases for weakly contrasted inserts and small discontinuities. For this reason, LPT should be regarded as a promising method for comparative defect detectability studies and rapid inspection of composite structures, while quantitative interpretation of defect size should be performed with caution, especially for small and low-contrast indications.

Taken together, these findings provide a basis for defining the operational envelope of LPT as applied to CFRP structures and highlight the importance of defect classification in any thermographic inspection campaign.

6. CONCLUSIONS

This study evaluated the applicability of LPT for detecting artificial defects in a CFRP laminate with variable thickness. The results demonstrated that LPT is capable of detecting several types of subsurface discontinuities, but its effectiveness depends strongly on defect type, nominal dimension and embedded depth. Flat-bottom holes filled with epoxy resin were the most detectable and the most repeatable defect class, while graphite foil remained undetected under the applied experimental conditions. Flat-bottom holes and paper inserts showed good but incomplete detectability, whereas prepreg foil was detected less frequently but was sized relatively accurately when visible. Detectability increased with increasing nominal defect dimension, and defects of 6 mm were generally below the robust detection limit of the applied configuration. The results also showed that accurate detection does not necessarily imply accurate sizing, since some defect classes were systematically overestimated or underestimated. Overall, the study confirms that LPT is a promising NDT method for the rapid inspection of CFRP structures, although its performance is limited for defects generating low thermal contrast and for small subsurface discontinuities.

Authors statement

All persons who meet authorship criteria are listed as authors, and all authors certify that they have participated sufficiently in the work to take public responsibility for the content, including participation in the concept, design, analysis, writing, or revision of the manuscript. This statement is signed by all the authors.

Acknowledgements

Funding: This work was supported by The National Centre for Research and Development, Poland (grant number 4/SZAFIR/2021, "Development of modern, breakthrough technologies for the security and defense of the state" p. "SZAFIR").

Data Availability

Some or all data, models, or code that support the findings of this study are available from the corresponding author upon reasonable request.

References

Alemour, B., Badran, O., & Hassan, M. R. (2019). A review of using conductive composite materials in solving lightning strike and ice accumulation problems in aviation. *Journal of Aerospace Technology and Management*, *11*, e1919. https://doi.org/10.5028/jatm.v11.1022

Almond, D. P., & Pickering, S. G. (2012). An analytical study of the pulsed thermography defect detection limit. *Journal of Applied Physics*, *111*, 093510.

Almond, D. P., Angioni, S. L., & Pickering, S. G. (2017). Long pulse excitation thermographic nondestructive evaluation. *NDT & E International*, *87*, 7–14. https://doi.org/10.1016/j.ndteint.2017.01.003

Balageas, D. L., & Roche, J. M. (2014). Common tools for quantitative pulse and step-heating thermography – Part I: Theoretical basis. *Quantitative InfraRed Thermography Journal*, *11*, 43–56.

Balageas, D., Maldague, X., Burleigh, D., Vavilov, V. P., Oswald-Tranta, B., Roche, J. M., Pradere, C., & Carlomagno, G. M. (2016). Thermal (IR) and other NDT techniques for improved material inspection. *Journal of Nondestructive Evaluation*, *35*, 18. https://doi.org/10.1007/s10921-015-0331-7

Carslaw, H. S., & Jaeger, J. C. (1959). *Conduction of heat in solids* (2nd ed.). Clarendon Press.

Deák, T., & Czigány, T. (2009). Chemical composition and mechanical properties of basalt and glass fibers: A comparison. *Textile Research Journal*, *79*(7), 645–651.

Favro, L. D., Han, X., Wang, Y., Kuo, P. K., & Thomas, R. L. (1995). Pulse-echo thermal wave imaging. *Review of Progress in Quantitative Nondestructive Evaluation*, *14*, 425–429. https://doi.org/10.1007/978-1-4615-1987-4_50

Ghadermazi, K., Khozeimeh, M. A., Taheri-Behrooz, F., & Safizadeh, M. S. (2015). Delamination detection in glass–epoxy composites using step-phase thermography (SPT). *Infrared Physics & Technology*, *72*, 204–209. https://doi.org/10.1016/j.infrared.2015.08.006

Huang, Z., Zhu, J., Zhuo, L., Li, C., Liu, C., Hao, W., & Xie, W. (2022). Non-destructive evaluation of uneven coating thickness based on active long pulse thermography. *NDT & E International*, *130*, 102672. https://doi.org/10.1016/j.ndteint.2022.102672

Kalyanavalli, V., Ramadhas, T. K. A., & Sastikumar, D. (2018). Long pulse thermography investigations of basalt fiber reinforced composite. *NDT & E International*, *100*, 84–91. https://doi.org/10.1016/j.ndteint.2018.08.007

Kamińska, P., Ziemkiewicz, J., Synaszko, P., & Dragan, K. (2019). Comparison of pulse thermography (PT) and step heating (SH) thermography in non-destructive testing of unidirectional GFRP composites. *Fatigue of Aircraft Structures*, *(11)*, 87–102.

Maldague, X. P. V. (2001a). Infrared and thermal testing. In P. O. Moore (Ed.), *Nondestructive testing handbook*. ASNT.

Maldague, X. P. V. (2001b). *Theory and practice of infrared technology for non-destructive testing*. John Wiley & Sons.

Manohar, A., & di Scalea, F. (2013). Determination of defect depth and size using virtual heat sources in pulsed infrared thermography. *Experimental Mechanics*, *53*(4), 661–671.

Pedrayes, O. D., Lema, D. G., Usamentiaga, R., Venegas, P., & García, D. F. (2022). Semantic segmentation for non-destructive testing with step-heating thermography for composite laminates. *Measurement*, *200*, 111653. https://doi.org/10.1016/j.measurement.2022.111653

Restrepo-Girón, A. D., & Loaiza-Correa, H. (2016). Background thermal compensation by filtering for contrast enhancement in active thermography. *Journal of Nondestructive Evaluation*, *35*, 20. https://doi.org/10.1007/s10921-016-0336-x

Ringermacher, H. I., Archacki, R. J., Jr., & Veronesi, W. A. (1998). *Nondestructive testing: Transient depth thermography* (US Patent 5,711,603). United States Patent and Trademark Office.

Roche, J. M., & Balageas, D. L. (2015). Common tools for quantitative pulse and step-heating thermography – Part II: Experimental investigation. *Quantitative InfraRed Thermography Journal*, *12*(1), 1–23.

Shepard, S. M. (2003). *Temporal noise reduction, compression and analysis of thermographic image data sequences* (US Patent 6,516,084). United States Patent and Trademark Office.

Sun, J. G. (2006). Analysis of pulsed thermography methods for defect depth prediction. *Journal of Heat Transfer*, *128*, 329–338.

Świderski, W., & Vavilov, V. (2009). Wyznaczanie termofizycznych charakterystyk materiałów metodami termografii w podczerwieni [Determination of thermophysical characteristics of materials using infrared thermography methods]. *Biuletyn Wojskowej Akademii Technicznej*, *58*(3), 149–168. (in Polish)

Vavilov, V. P., & Burleigh, D. D. (2015). Review of pulsed thermal NDT: Physical principles, theory and data processing. *NDT & E International*, *73*, 28–52.

Vedula, S. (2010). *Infrared thermography and ultrasonic inspection of adhesive bonded structures: Overview and validity* [Master's thesis, Clemson University].

Wang, Z., Tian, G. Y., Meo, M., & Ciampa, F. (2018). Image processing based quantitative damage evaluation in composites with long pulse thermography. *NDT & E International*, *99*, 93–104.

Wang, Z., Wan, L., Zhu, J., & Ciampa, F. (2022). Evaluation of defect depth in CFRP composites by long pulse thermography. *NDT & E International*, *129*, 102658.

Zhuo, L., Yang, X., Zhu, J., Huang, Z., Chao, J., & Xie, W. (2023). Size determination of interior defects by reconstruction of subsurface virtual heat flux for step heating thermography. *NDT & E International*, *133*, 102734.